Infrared Plasmonics of Al-Mn Codoped ZnO and In-M (M = Fe and Mn) Codoped CdO Nanocrystals

A THESIS SUBMITTED IN PARTIAL FULFILMENT OF THE REQUIREMENTS FOR THE DEGREE

of BS-MS dual degree

by

ASWATHI ASHOK

(Reg. No. 20101042)

IISER PUNE

Thesis supervisor

DR. ANGSHUMAN NAG

DEPARTMENT OF CHEMISTRY

INDIAN INSTITUTE OF SCIENCE EDUCATION AND RESEARCH (IISER), PUNE

CERTIFICATE

This is to certify that this dissertation entitled **Infrared Plasmonics of Al-Mn Codoped ZnO and In-M (M = Fe and Mn) Codoped CdO Nanocrystals** towards the partial fulfilment of the BS-MS dual degree programme at the Indian Institute of Science Education and Research (IISER), Pune represents original research carried out by **Aswathi Ashok** at IISER Pune under the supervision of Dr. Angshuman Nag, Ramanujan Fellow, Department of Chemistry during the academic year 2014-2015.

Pune

25.03.2015

Angshuman Nag

Dr. Angshuman Nag

(Supervisor)

DECLARATION

I hereby declare that the matter embodied in the report entitled **Infrared Plasmonics of Al-Mn Codoped ZnO and In-M (M = Fe and Mn) Codoped CdO Nanocrystals** are the results of the investigations carried out by me at the Department of Chemistry, Indian Institute of Science Education and Research (IISER), Pune, under the supervision of Dr. Angshuman Nag and the same has not been submitted elsewhere for any other degree.

Pune

25.03.2015

Aswathi Ashok

(Reg. No. 20101042)

ACKNOWLEDGEMENT

CONTENTS

LIST OF FIGURES

ABSTRACT

Plasmonic properties in semiconductor nanocrystals have been an attracting area of research in recent years. Transparent conducting oxides (TCOs) like Al doped ZnO nanocrystals and indium doped cadmium oxide are semiconductor materials which show interesting plasmonic properties in the near to mid-IR region. Herein, we try to synthesize Al and Mn codoped ZnO nanocrystals and In and M (M= Fe and Mn) codoped CdO NCs to invoke plasmonic as well as magnetic properties simultaneously. We report AZO nanocrystals which exhibit plasmonic properties at wavelength longer than 2000 nm. We could also obtain In-Mn codoped CdO nanocrystals and In-Fe codoped CdO nanocrystals with plasmonic peaks in near-IR to mid-IR region. Effect of doping magnetic ions (Mn^{2+} and Fe^{3+}) on plasmonic properties has been studied.

1. <u>INTRODUCTION</u>

Localized surface plasmon resonance or LSPR, is an optical phenomenon in which the free electrons on the surface of a nanoparticles collectively oscillate when they interact with an incoming electromagnetic radiation. LSPR from metal nanocrystals (NCs) has been widely studied over the past few years.[1] Recent researches show that LSPR is also exhibited by semiconductor nanocrystals.[2,3] The LSPR absorption is largely dependent upon the free electron concentration of the material. LSPR peaks can also arise from equilibrium steady state population of doped semiconductors, and from photo-excited undoped semiconductors.[4] Figure 1 is a schematic that explains the production of LSPR bands in photo excited ZnO nanocrystals.[4]
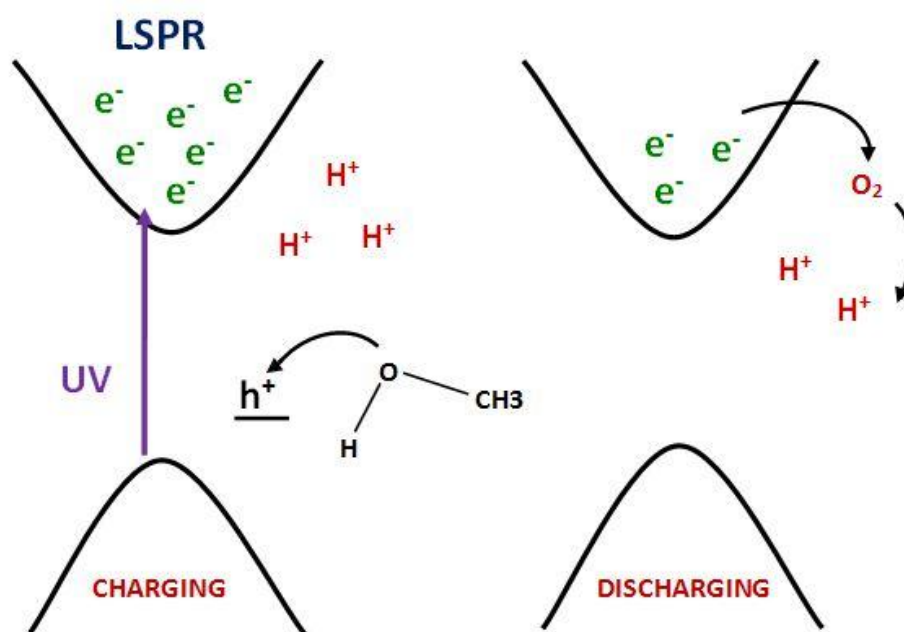
Figure 1: Schematic of charging of ZnO nanocrystals by irradiation of UV light. Discharging takes place when the electrons are exposed to oxygen (adapted from reference 4).

When a nanomaterial is irradiated with a photon of energy greater than or equal to the band gap, the electrons in the valence band get excited to the conduction band producing an electron hole pair. The hole scavengers remove the hole from the valence band and release protons in solution. Hence the free electrons in the conduction band give rise to LSPR.[4] But this is an excited state process which

occurs only in the absence of electron scavengers like oxygen. Hence the practical application of photo excited LSPR is limited. But in the case of semiconductor oxides doping can provide free electrons in the conduction band giving rise to LSPR. TCOs are such semiconductor material whose free electron concentration can be varied by doping with different concentrations of an aliovalent ion.[5] The LSPR frequency is also tunable by the size and geometry of the NCs as well as by the local medium to some extent .[6]

1.1.   Drude model to explain LSPR

Drude model of electrical conduction explain the transport properties of electrons in a material. It assumes that a metal is composed of a collection of positively charged ions from which some free electrons are separated. It neglects any long range interaction between the electrons and the ions. The properties of a metal are dependent upon these free electrons.[7] When the frequency of incident electromagnetic radiation matches with the natural frequency of these free electrons on the surface, it gives rise to a LSPR band. The localized surface plasmons enhance the electric field near the surface of the nanoparticles and this enhancement disappears quickly while moving away from the surface. The LSPR frequency is given by the following equation.

$$\omega_{sp} = \sqrt{\frac{N_c e^2}{(\varepsilon_\infty + \varepsilon_m)\varepsilon_o m_c} - \gamma^2} \qquad (1)$$

Where,

ω_{sp} = LSPR frequency

N_c = free carrier density

γ = bulk collision frequency

ε_o = absolute permittivity of air/vacuum

ε_m = dielectric constant of the medium

ε_∞ = dielectric constant at high frequency

m_c = effective mass of the carrier

e = electronic charge

Drude model which was initially applicable for metal NCs, it can also be used to explain the free carrier concentration in semiconductor NCs having size much greater than the De Broglie wavelength of the carrier. The model is not applicable to smaller NCs since it could not explain scattering and carrier localization in NCs having diameter less than the Bohr exciton radius.[8] Hence semiconductor NCs should also require a quantum mechanical explanation for free carrier densities.[9] Metal NCs having high free electron concentration exhibit LSPR in visible region of electromagnetic spectrum whereas doped semiconductor NCs with fewer free electrons show LSPR in near to mid IR regime.[10]

1.2. <u>Transparent conducting oxides (TCOs)</u>

TCOs are materials that are electrically conductive and at the same time optically transparent to visible light. Sn-doped In_2O_3 (ITO), Al-doped ZnO (AZO), In-doped CdO (ICO) etc are some of the famous TCOs which exhibit strong plasmonic absorption in NIR region.[11-13] The tunability of free electron concentration in TCO will give rise to tunable LSPR bands in near IR and mid IR regions. Researchers are giving great importance to the study of TCOs since the simultaneous exhibition of electrical conductivity and visible light transparency can be utilized for various applications in optoelectronics. The first TCO CdO was reported way back in 1907 by Badeker et. al. CdO has got great attention due to its high electron mobility. 50 years after the discovery, TCOs started getting significant progress in day-to-day applications. ITO is one of the widely used TCOs having LSPR in NIR to mid-IR region.[14,15] Limited earth abundance and thus the high cost of ITO demanded the need for a cheaper TCO. Even though CdO based TCOs exhibit high electrical conductivity most work avoid the use of Cd due to toxicity concerns. Among the existing TCOs ZnO has got much attention due to its less toxicity, earth abundance and high chemical stability.[11] ZnO having band gap energy of 3.3 eV has found wide range of applications in optoelectronics and spin based devices. n-type doping with Al, Ga, In etc has been reported to enhance the free electron concentrations in the conduction band leading to higher electrical conductivity and strong plasmonic absorption. Studies show that room temperature ferromagnetism can also be

achieved in TCOs by doping transition metals like Fe.[16,17] D.J. Milliron et.al reported the synthetic procedure of AZO NCs by controlling the size and doping simultaneously.[11] Al doping is favoured in ZnO lattice due to the similar ionic radii and electronegativities of Al and Zn. On the other hand, doping with different elements such as In, Sn, Ti, Zn, Al and F to CdO lattice enables tuning of optical and electronic properties. Among such dopants, In doping is given prior importance due to the similar ionic radii of both Cd and In. The 5s orbital of In mixes with the 5s orbital of Cd, lowering optical absorption of the NCs. In the previous year, the first synthesis of ICO via a high temperature surfactant assisted approach was reported.[13] It has been shown to have the highest electrical conductivity reported compared to all other commercial TCOs.[18] Morphology of the NCs can be tuned by varying ligand concentration and reaction temperature.

Our work mainly deals with achieving simultaneous plasmonic and magnetic properties in AZO and ICO by codoping. We try to synthesize Al-Mn codoped ZnO and In-Mn and In-Fe codoped CdO in solution so that we may obtain magnetic properties along with plasmonic properties in NIR region. Such multifunctionality can be utilized for various applications like magnetic imaging and photothermal therapy .[5]

2. __METHODS__

All synthesis are performed using standard Schlenk line techniques under inert atmosphere.

2.1. __Preparation of AZO nanocrystals:__

__Chemicals:__

The following chemicals are used to synthesize AZO NCs. Zinc acetyl acetonate, aluminium acetyl acetonate (99%), oleic acid (90%) (OLAC), 1,2- hexadecanediol (90%), 1-octadecene (90%) (1-ODE), ethanol, hexane, tetrachloroethylene (TCE). All are purchased from Sigma Aldrich.

Synthesis:

A solution containing zinc acetyl acetonate (1 mmol), aluminium acetyl acetonate (0.1 to 0.5 mmol), oleic acid (6 mmol), 1, 2- hexadecanediol (5 mmol) and 15 ml octadecene were taken in a three-necked flask. The solution was kept at 100^0C under nitrogen atmosphere for 1 hr. The temperature is then increased slowly to 240^0C. The reaction mixture was allowed to cool after 5 hrs of uniform heating. The nanocrystals were precipitated using ethanol and separated using centrifugation at 7500 rpm for 10 minutes. The NCs were redispered in hexane (1 ml). After two cycles of redispersion and reprecipitation, the NCs were collected and dispersed in a suitable non polar solvent. Undoped ZnO NCs were obtained by following the same procedure without the addition of aluminium precursor.[11]

2.2. Preparation of In-Mn and In-Fe codoped CdO nanocrystals:

Chemicals:

The following chemicals were used in the synthesis of ICO NCs. Cadmium (II) acetyl acetonate (99.9%), indium (III) acetate, manganese (II) acetyl acetonate, iron (III) acetyl acetonate, oleic acid (90%) (OLAC), 1-octadecene (90%), ethanol, toluene, carbon tetrachloride (CCl_4). All are purchased from Sigma Aldrich.

Synthesis:

 A solution containing cadmium (II) acetyl acetonate (0.95 - 0.80 mmol), indium (III) acetate (0.05 - 0.20 mmol), OLAC (2-4 mmol) and 15 ml 1-octadecene were taken in a three-necked flask and evacuated at 120^0C for 1 hour under nitrogen-hydrogen atmosphere (hydrogen 10%). The reaction is heated quickly to 300^0C. The reaction is allowed to cool after the color change from brown to dark green. The solution is washed with ethanol followed by centrifugation at 7500 rpm for 10 minutes. The NCs were redispersed in toluene. Undoped CdO was prepared following the same procedure without the addition of indium precursor. All the NCs were dispersed in a suitable nonpolar solvent. They settle overtime after 4 to 5 hours.[13] Manganese and iron doped ICO were also synthesised using manganese (II) acetyl acetonate and iron (III) acetyl acetonate respectively.

3. <u>RESULTS AND DISCUSSIONS</u>

<u>Nanocrystal characterization:</u>

The AZO and ICO nanocrystals obtained using solution processed synthesis technique were analysed using powder X-ray diffraction (PXRD), UV-Vis-NIR absorption spectroscopy.

3.1. <u>UV/Vis/NIR absorption spectroscopy</u>

UV/Vis/NIR absorption spectra of AZO and ICO NCs were obtained using LAMBDA 950 UV/Vis/NIR spectrometer (PerkinElmer) in tetrachloroethylene (TCE) and carbon tetrachloride (CCl_4) respectively.

3.1.1. <u>Absorption spectra of AZO NCs</u>:

The NIR absorption spectra of AZO NCs were obtained in tetrachloroethylene (TCO). The UV/Vis/NIR absorption analysis of AZO NCs with different Al content showed a broad absorption peak at wavelength longer than 2000 nm (fig.2). As the percentage of Al doping increased from 5 % to 15 % the absorbance in NIR region also increased. Further Al doping caused a reduction in plasmonic absorption. The LSPR absorption is highly dependent upon the amount of doping. Above 15 % there is no more increase in the free electron concentration in ZnO conduction band. Higher levels of doping may result in electrons to get scattered or trapped by the Al centres. Hence there will be no more increase in plasmonic absorption. There is an increase in optical band gap of the NCs on increasing the amount of doping (fig. 3). The band gap of AZO NCs falls in the range of 3.4 to 3.8 eV as the amount of doping is increased. When the extent of doping is increased more and more states in conduction band will be populated which results in the increase in bandgap of the material which is referred to as Burstein shift. When all states near the conduction band is populated the absorption peak shifts towards higher energy resulting in increase in optical band gap.
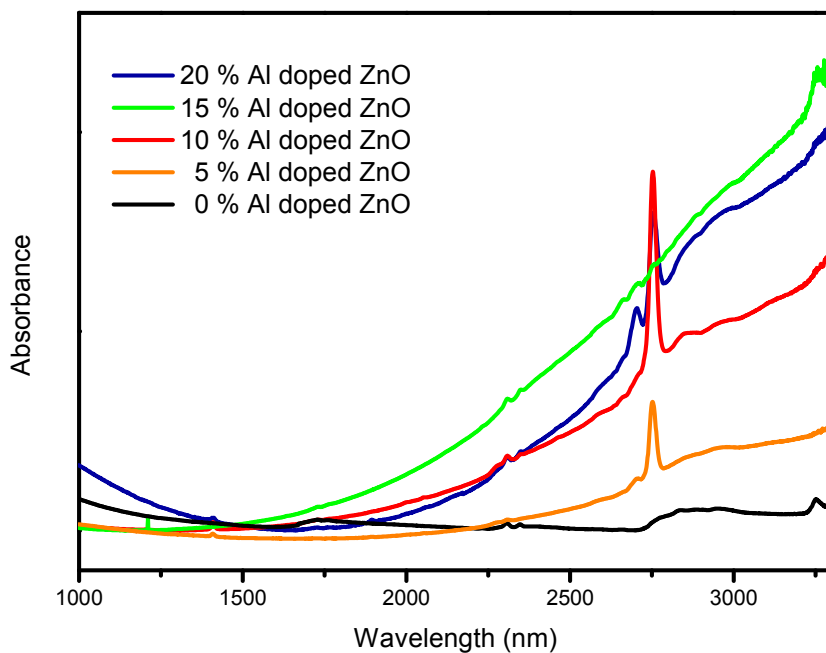
Figure 2: Absorption spectra of Al-doped ZnO NCs with different Al doping levels
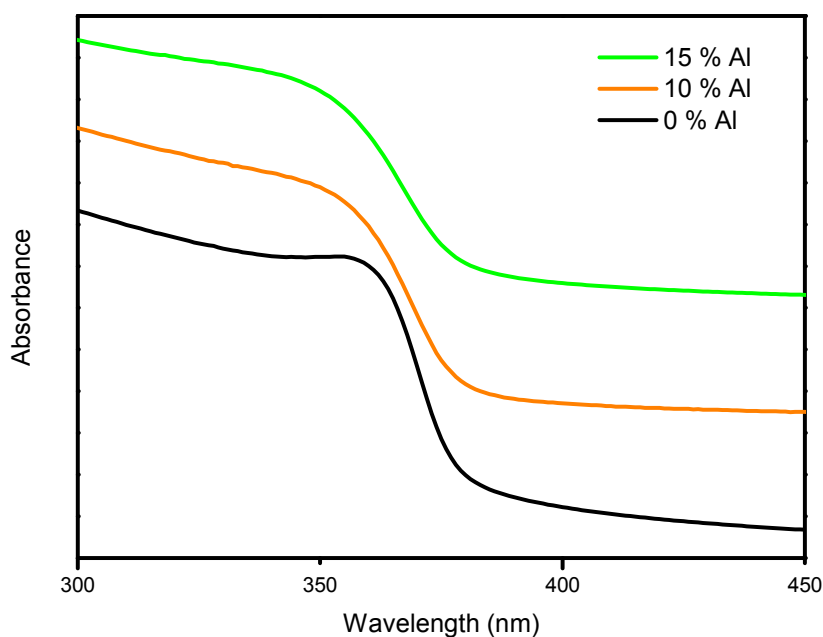

Figure 3: Absorption spectra of Al-doped ZnO NCs showing shift in optical band gap.

3.2.1. <u>Absorption spectra of In-Mn and In-Fe codoped CdO NCs</u>

The absorption spectra of In-Mn and In-Fe codoped CdO NCs were obtained in tetrachloroethylene (CCl_4). The plasmonic character of ICO NCs is extremely

dependent upon oleic acid concentration. There is minimum or no absorption in NIR region for OLAC concentration more than 5 mmol. Maximum absorbance is shown by 15 % ICO nanocrystals. In both the NCs a broad peak is observed at wavelength longer than 1500 nm. As the amount of codopant concentration is increased, the absorbance peak is red shifted. When the percentage of Mn doping is increased from 1% to 10 % we could observe a decrease in absorbance (fig. 4). When a In^{3+} ion is replaced by a Mn^{2+} ion a hole is created thereby reducing the free electron concentration. This may be the reason for the reduction in absorbance when the amount of dopant is increased. In the case of In-Fe codoped CdO NCs even though we expect a red shift, the absorption peak is a blue shifted in for 1 % Fe doping compared to 0 % Fe doping (fig. 5). However the trend in variation of plasmonic properties in our NCs is not properly understood yet. We are trying to optimize the reaction conditions inorder to obtain a proper LSPR band.
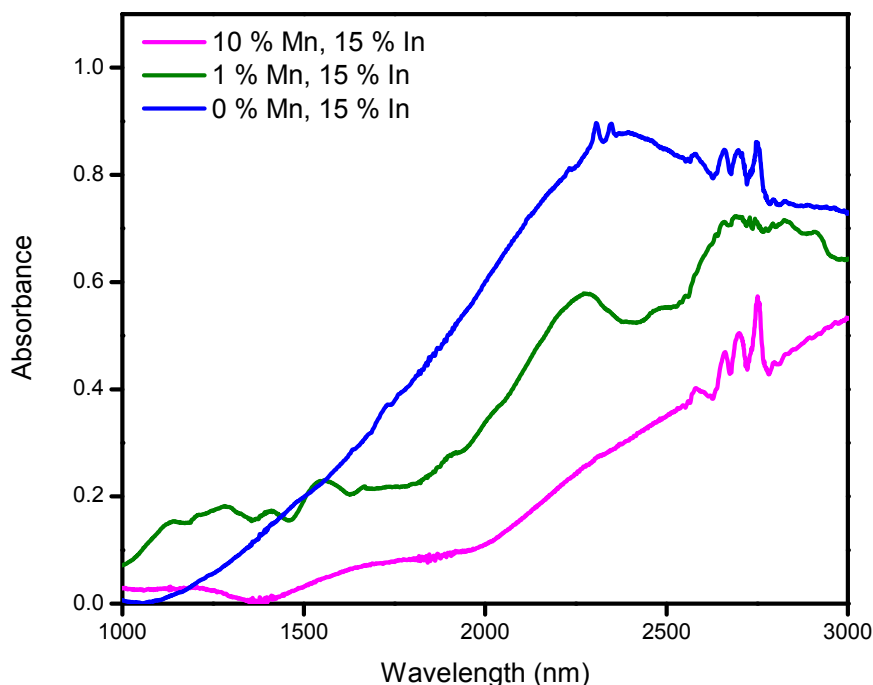

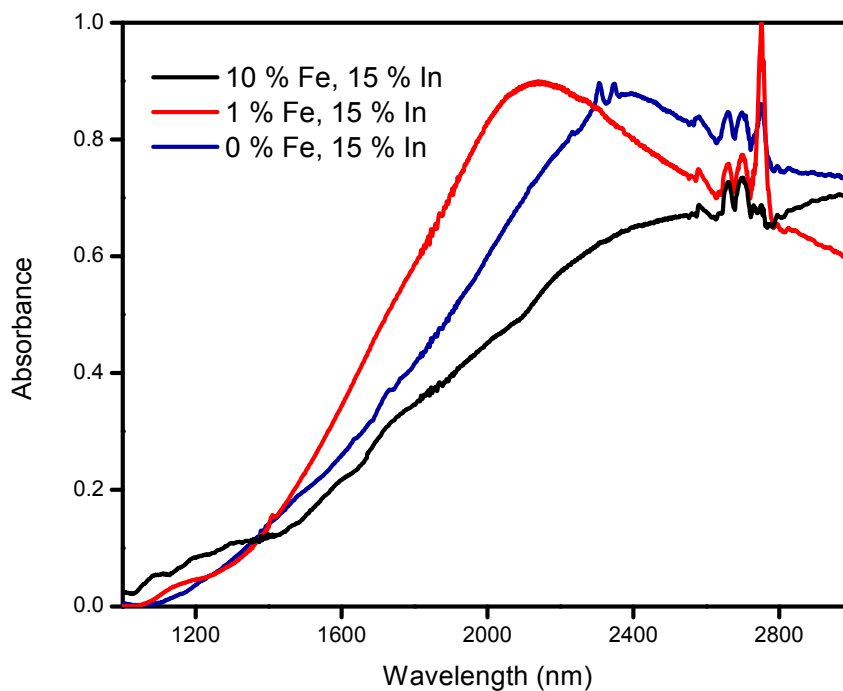Figure 4: Absorption spectra of In-MN codoped CdO NCs with different Mn doping levels

Figure 5: Absorption spectra of In-Fe codoped CdO NCs with different Fe doping levels.

3.2. <u>Powder X-ray diffraction (PXRD)</u>

The AZO and ICO powders were characterised using Bruker D8 ADVANCE powder X-ray diffractometer. X-ray diffraction technique is most commonly used for phase identification. Crystal structure and size can also be determined using this technique.

3.2.1. <u>PXRD of AZO NCs:</u>

Inorder to study the effect of dopant incorporation in AZO NCs were analysed by powder X-ray diffraction studies. All doping levels showed wurtzite crystal structure. No other impurity peaks were observed. Diffraction patterns each AZO NCs with different Al doping levels showed a slight shift towards larger 2 theta values indicating Al incorporation in ZnO lattice (fig.6). As the percentage of aluminium doping increases, the shift towards larger 2 theta values also increases.
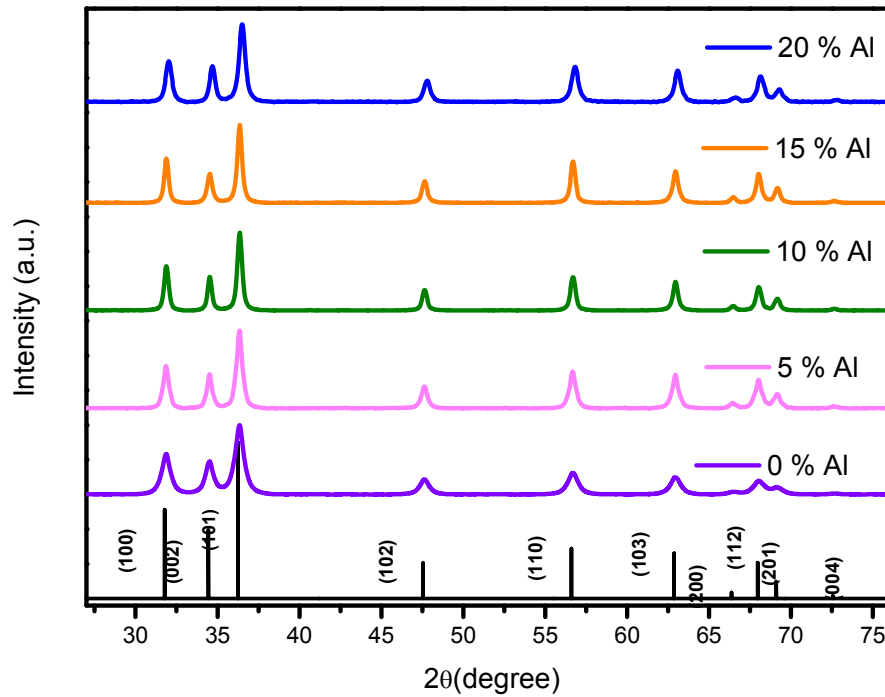
Figure 6: PXRD patterns of AZO NCs with different Al content. The reference diffraction pattern of bulk wurtzite ZnO is shown at the bottom (ICSD-75-0576).

This shift can be explained using Bragg equation.

$$n\lambda = 2dsin\theta \qquad (2)$$

Where,

n = positive integer

λ = wavelength of incident light

d = interplanar distance

θ = scattering angle

The ionic radii of Al^{3+} ions (67.5pm) is smaller than that of Zn^{2+} ions (88pm). Hence when Zn^{2+} ions are replaced by Al^{3+} ions the lattice size decreases and as a result the interplanar distance (d) decreases. So according to equation 2, the diffraction peaks shift towards larger 2 theta values.

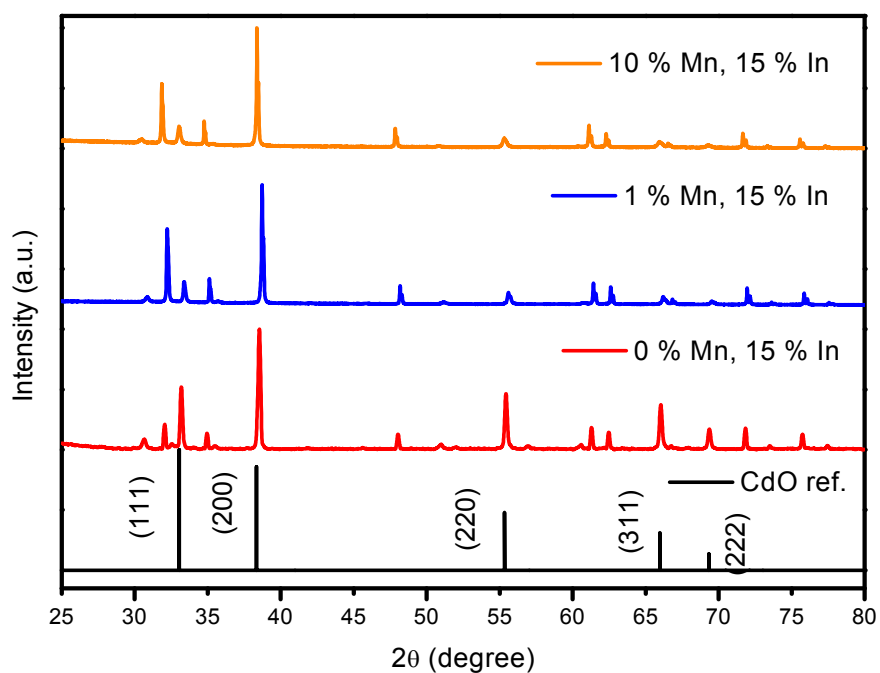### 3.2.2. <u>PXRD of Mn and Fe doped CdO NCs:</u>

Figure 7: PXRD patterns of In-Mn codoped CdO NCs with different Mn doping. The reference diffraction pattern of bulk FCC CdO is shown at the bottom (ICSD- 065-2908).
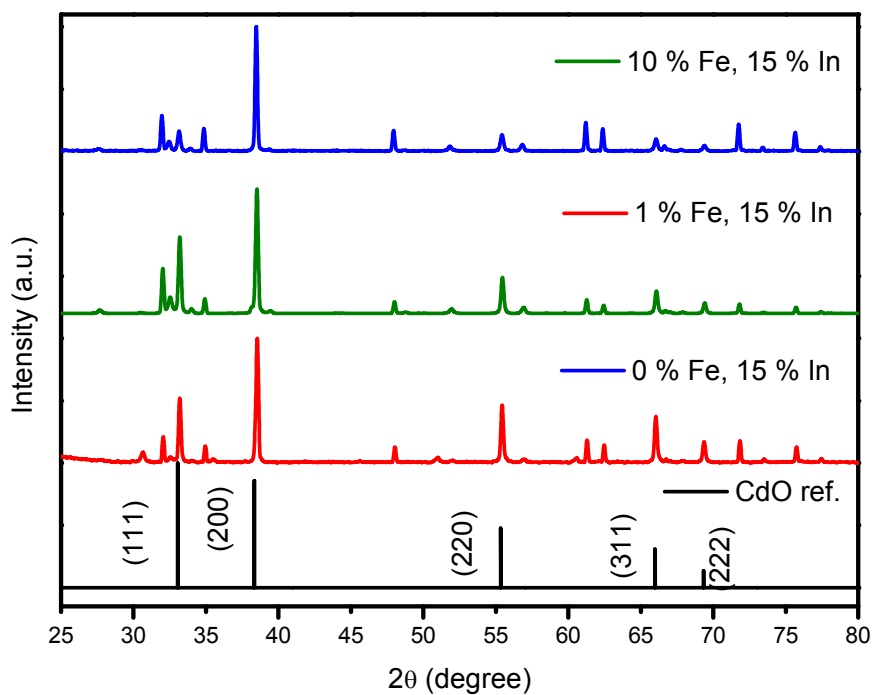

Figure 8: PXRD patterns of In-Fe codoped CdO NCs with different Fe doping. The reference diffraction pattern of bulk FCC CdO is shown at the bottom (ICSD- 065-2908).

The PXRD patterns of Mn and Fe doped ICO NCs have a fcc crystal structure. However the patterns also showed peaks of indium oxide and cadmium indium oxide which indicates that the NCs were not phase pure. Mn and Fe incorporation in ICO NCs were analysed using diffraction studies. Shift in position of peaks is observed in both Mn doped ICO diffraction pattern as well as Fe doped ICO diffraction pattern. Both the PXRD patterns show shift in peak positions towards larger 2 theta values consistent with Mn and Fe doping. The ionic size of Mn^{2+} (83 pm) and Fe^{3+} (64.5pm) is smaller than that of Cd^{2+} (109 pm). Hence the interplanar distance decreases and the scattering angle increases following Bragg equation.

The average size of the AZO NCs was calculated using Debye-Scherer formula.

$$\tau = \frac{k\lambda}{\beta cos\theta} \qquad (3)$$

Where,

τ = average size of the crystalline domain

k = shape factor which is normally taken as 0.9

λ = wavelength of X-ray

β = line broadening at half the maximum intensity (FWHM) in radians.

θ = Bragg angle.

The average size of AZO NCs obtained using equation 3 is around 26 nm.

Similarly average size of Mn and Fe doped ICO NCs were also calculated by the same way. The average size obtained for Mn and Fe doped ICO NCs is around 47 nm and 36 nm respectively.

4. <u>CONCLUSION AND FUTURE PLANS</u>

AZO and In-M (M=Fe and Mn) doped CdO NCs show plasmonic peaks in near to mid IR region. We were able to obtain AZO NCs having average size of 26 nm which shows plasmonic peak having wavelength longer than 2000 nm. The plasmonic absorbance increases by increasing the amount of Al-doping in AZO NCs because of the increase in free electron concentration. We could observe maximum absorbance for 15 % AZO. Further increase in percentage doping of Al reduces the absorbance since the free electrons get trapped in Al centres. In-Mn as well as In-Fe codoped CdO also showed absorption in mid-IR region. Red shift is observed in In-Mn codoped CdO NCs as we increase the dopant concentration. The reason behind the plasmonic behaviour in In-M codoped NCs is not exactly understood.

The variation of plasmonic properties according to dopant incorporation has to be studied further. Codoped AZO NCs with Mn has to be analysed to ensure that magnetic and plasmonic properties can be achieved simultaneously. Further studies have to be undertaken giving more emphasize to electrical conductivity measurements. TEM images of the NCs are yet to be obtained to have estimation about the exact size and shape of these nanocrystals.

5. <u>REFERENCES</u>

(1)   El-Sayed, M. A. *Acc. Chem. Res.* **2001**, *34*, 257.

(2)   Lounis, S. D.; Runnerstrom, E. L.; Llordés, A.; Milliron, D. J. *J. Phys. Chem. Lett* **2014**, *5*, 1564.

(3)   Faucheaux, J. A.; Stanton, A. L. D.; Jain, P. K. *T J.Phys. Chem. Lett.* **2014**, *5*, 976.

(4)   Faucheaux, J. A.; Jain, P. K. *J. Phys. Chem. Lett.* **2013**, *4*, 3024.

(5)   Tandon, B.; Shanker, G. S.; Nag, A. *J. Phys. Chem. Lett.* **2014**, *5*, 2306.

(6)   Luther, J. M.; Jain, P. K.; Ewers, T.; Alivisatos, A. P. *Nat Mater* **2011**, *10*, 361.

(7)   Alvarez, M. M.; Khoury, J. T.; Schaaff, T. G.; Shafigullin, M. N.; Vezmar, I.; Whetten, R. L. *J. Phys. Chem. B* **1997**, *101*, 3706.

(8)   Schimpf, A. M.; Thakkar, N.; Gunthardt, C. E.; Masiello, D. J.; Gamelin, D. R. *ACS Nano* **2014**, *8*, 1065.

(9)   Nütz, T.; Felde, U. z.; Haase, M. *J. Chem.Phys..* **1999**, *110*, 12142.

(10)   Liong, M.; Lu, J.; Kovochich, M.; Xia, T.; Ruehm, S. G.; Nel, A. E.; Tamanoi, F.; Zink, J. I. *ACS nano* **2008**, *2*, 889.

(11)   Buonsanti, R.; Llordes, A.; Aloni, S.; Helms, B. A.; Milliron, D. J. *Nano Letters* **2011**, *11*, 4706.

(12)   Della Gaspera, E.; Chesman, A. S. R.; van Embden, J.; Jasieniak, J. J. *ACS Nano* **2014**, *8*, 9154.

(13)   Gordon, T. R.; Paik, T.; Klein, D. R.; Naik, G. V.; Caglayan, H.; Boltasseva, A.; Murray, C. B. *Nano Letters* **2013**, *13*, 2857.

(14)   Kanehara, M.; Koike, H.; Yoshinaga, T.; Teranishi, T. *J. Am. Chem. Soc.* **2009**, *131*, 17736.

(15)   Li, S. Q.; Guo, P.; Zhang, L.; Zhou, W.; Odom, T. W.; Seideman, T.; Ketterson, J. B.; Chang, R. P. H. *ACS Nano* **2011**, *5*, 9161.

(16)   Farvid, S. S.; Ju, L.; Worden, M.; Radovanovic, P. V. *J. Phy. Chem. C* **2008**, *112*, 17755.

(17)   Singhal, A.; Achary, S. N.; Manjanna, J.; Jayakumar, O. D.; Kadam, R. M.; Tyagi, A. K. *J. Phy. Chem. C* **2009**, *113*, 3600.

(18)   Yan, M.; Lane, M.; Kannewurf, C. R.; Chang, R. P. H. *Appl. Phys. Lett.* **2001**, *78*, 2342.